

Brownian Dynamics Simulations of the Growth of Metal Nanocrystal Ensembles on Electrode Surfaces in Solution: 2. The Effect of Deposition Rate on Particle Size Dispersion[†]

Reginald M. Penner*

Department of Chemistry, University of California, Irvine, Irvine, California 92679-2025

Received: April 6, 2001; In Final Form: July 6, 2001

An adaptation of the Brownian dynamics simulation method has been used to model the growth of a particular 200-particle ensemble of silver nanoparticles. This ensemble of particles was randomly positioned on an electrode of total area $1.0 \times 10^{-9} \text{ cm}^2$, and these particles possessed a significant size distribution. The growth of this distribution was investigated at overpotentials ranging from -1 mV to -200 mV . These simulations demonstrate that reduced rates of electrodeposition effectively reduce the particle size dispersion present in an ensemble of particles. The beneficial effect of “slow growth” is brought about by the elimination or reduction of the diffusional coupling present between neighboring particles on the electrode surface.

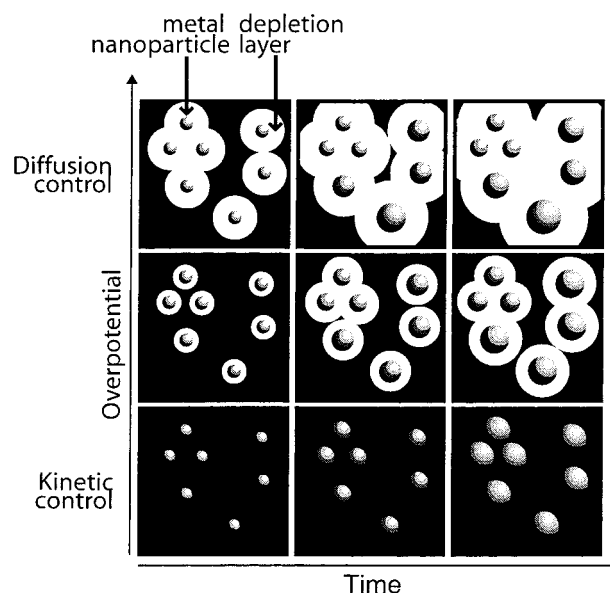
I. Introduction

In this paper I report the results of Brownian dynamics simulations for the growth of metal nanoparticle ensembles on electrode surfaces. Specifically, the growth of an ensemble of 200 silver nanoparticles has been investigated over a wide range of deposition overpotentials ($\eta_{\text{dep}} = E_{\text{dep}} - E_{\text{eq}}$) down to $\eta_{\text{dep}} = -1.0 \text{ mV}$. These simulations provide clear evidence that slow electrodeposition rates are superior to growth at diffusion control if the objective is to minimize particle size dispersion. The context and motivation for this study are summarized in the following paragraphs.

Previously,^{1–5} we have demonstrated that at highly oriented pyrolytic graphite electrode surfaces, metal nanoparticles may be electrodeposited from dilute, aqueous solutions using large deposition overpotentials, but the size dispersion of these particles increases rapidly with deposition time. For example, in the case of platinum nanoparticle deposition at $\eta_{\text{dep}} = -500 \text{ mV}$, as particles were grown from a mean diameter of 2.6 nm (using a deposition time, $t_{\text{dep}} = 10 \text{ ms}$) to 7.2 nm ($t_{\text{dep}} = 100 \text{ ms}$), the relative standard deviation of the particle diameter ($\text{RSD}_{\text{dia}} = \sigma_{\text{dia}}/\langle \text{dia} \rangle$) increased from 35% ($\sigma_{\text{dia}} = 0.9 \text{ nm}$) to 44% ($\sigma_{\text{dia}} = 3.2 \text{ nm}$).⁵ It is impossible to grow dispersions of metal particles larger than 10 nm in diameter having any degree of size monodispersity under these conditions. Why? The heterogeneity of electrodeposited structures (of all types) is often attributed to progressive nucleation. This is particularly true when electrodeposited structures are observed to become increasingly heterogeneous with increasing deposition time. But progressive nucleation is not responsible for the particle size heterogeneity seen in our experiments because in these experiments there is clear experimental evidence for instantaneous⁶ nucleation.⁵ Since nucleation cannot be responsible for particle size heterogeneity, it must be concluded that the growth rates of individual platinum particles on these surfaces are dissimilar.

To elucidate the source of this “deposition rate dispersion”, we performed Brownian dynamics simulations of the growth

SCHEME 1: Depiction of the Effect of Interparticle Diffusion Coupling (or IDC) on Particle Size Dispersion at Three Deposition Rates



of silver particle ensembles.⁷ These simulations showed that, provided nucleation on the surface was spatially random, the size heterogeneity of silver particles increased as a function of time, even though these particles nucleated instantaneously. In fact, the rate at which σ_{dia} increased in these simulations ($d\sigma_{\text{dia}}/dt = 0.1 \text{ nm/ms}$)⁷ agreed well with the rate seen previously in the platinum deposition experiments.⁵ In contrast, particles that were located in a hexagonal array became more size-similar with deposition time.⁷ Moreover, the simulations revealed the existence of a correlation between the radii of two nearest neighbors, and the distance separating them on the electrode surface. On average, the closer a particle to its nearest neighbor, the smaller the mean diameter of these two particles relative to the mean for all of the particles on the surface.⁷ As shown in Scheme 1 (top), this “interparticle diffusion coupling” (or IDC) occurs when the depletion layers surrounding neighboring metal

[†] Part of the special issue “Royce W. Murray Festschrift”.

* Correspondence to: rmpenner@uci.edu.

particles overlap, thereby depressing the growth rates of these particles relative to that for metal particles growing in isolation on the surface. The elimination of IDC should make it possible to electrodeposit metal particle ensembles exhibiting improved size uniformity. How might this be accomplished?

Since the depletion layer surrounding each particle mediates IDC, elimination of this layer should eliminate IDC. One means for accomplishing this is shown in Scheme 1. The steady-state concentration of metal ions near a growing metal particle is given by:

$$C(R) = C^* - \frac{[C^* - C_0]r_0}{R} \quad (1)$$

where C^* is the bulk concentration of metal ions, r_0 is the electrode radius, R is the radial distance from the surface of the particle, and C_0 is the concentration at r_0 . If the depletion layer radius, r_d , is taken to be the radius at which the concentration in the depletion layer equals $0.95C^*$, an expression for r_d can be derived from eq 1:⁸

$$r_d = \frac{(C^* - C_0)r_0}{0.05C^*} \quad (2)$$

It is apparent from eq 2 that r_d is directly proportional to the quantity $C^* - C_0$. In principle, then, we wish to increase C_0 from 0 (corresponding to diffusion-controlled growth) to C^* (corresponding to kinetically controlled growth). Now $C_0 = C^*$ cannot be experimentally achieved for systems where the metal deposition reaction is reversible; however, this ideal is approached at slow growth rates. We hypothesized that slow growth (obtained using small values of η_{dep} below -75 mV) would lead to narrower particle size dispersions for electrodeposited metal particles on graphite, and we tested this hypothesis experimentally for silver⁸ and a variety of other metals.⁹ The conclusion of these experimental studies is that slow growth works extremely well. One example: The size distribution for $2 \mu\text{m}$ diameter silver particles prepared by slow growth exhibited a RSD_{dia} of 6% ($\sigma_{\text{dia}} = 0.12 \mu\text{m}$).

The Brownian dynamics simulations reported in this, the second paper on this subject from this laboratory, are intended to lead to a deeper understanding of slow growth. Specifically, this study addresses the following questions: (i) *Are the benefits of slow growth manifested in the Brownian dynamics results?* Do the benefits of slow growth derive from the transport physics of this problem or are chemical factors that are not included in the simulation important? (ii) *How effective is slow growth for minimizing particle size dispersion?* Specifically, is it possible to achieve convergent growth (RSD_{dia} decreasing with $\langle \text{dia} \rangle$) using this strategy? Convergent growth has not been seen in the experimental studies performed so far. (iii) *Does an optimum slow growth rate and η_{dep} exist?* Is there a threshold value for η_{dep} below which no further benefit is obtained? (iv) *What happens to an ensemble of size heterogeneous metal nanoparticles that is subjected to slow growth?* Does IDC persist even at extremely low growth rates?

II. The Mechanics of the Simulation

Each simulation involved the growth of the same ensemble of 200 hemispherical silver particles. These particles shown as points in Scheme 2, were randomly distributed on the electrode surface and they possessed a size distribution that was generated by growing the ensemble from initial radii of 2×10^{-8} cm (0.20 nm) to a final mean radius of 1.43×10^{-7} cm (1.43 nm) under

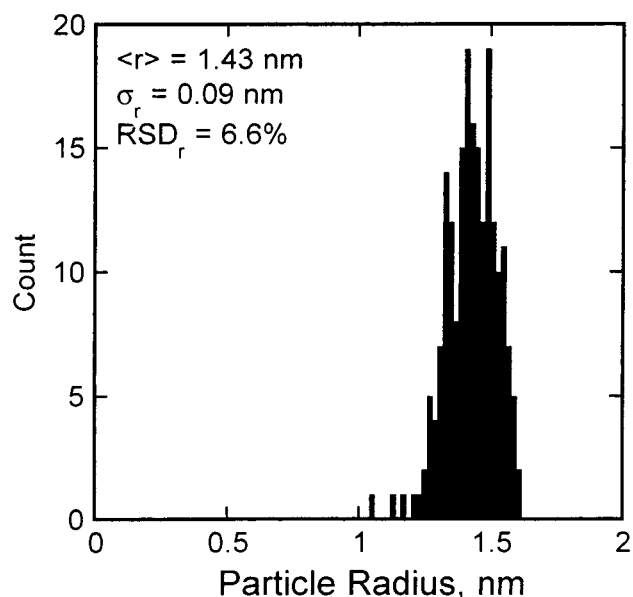
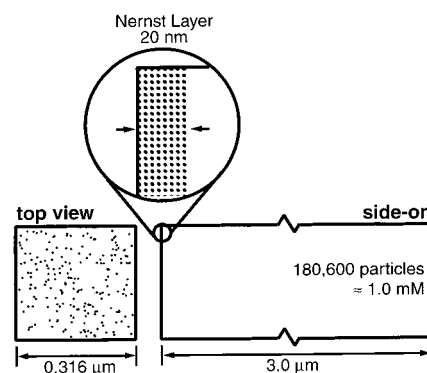


Figure 1. Size distribution for the 200 particle ensemble that served as the starting point for all of the simulations reported here.

SCHEME 2: The Simulation Box Employed in These Brownian Dynamics Simulations



conditions of diffusion control. The size distribution of the 200 particles used as the starting point for these simulations is shown in Figure 1.

From the starting point represented by the histogram of Figure 1, this 200 particle ensemble was grown from a 1×10^{-3} M "solution" of 180 660 "ions" in the rectangular cell (volume = 0.30 pL) shown in Scheme 1. These silver ions were modeled as points and were uniformly distributed within the rectangular simulation cell. Periodic boundary conditions were employed, and the transport of ions in the simulation was by diffusion only; the contributions of electromigration or diffusiomigration to the transport of the silver ions were neglected. The Brownian motion of each ion was generated using a modification of the algorithm of McCammon¹⁰ in which the Gaussian distributed random number used in his work was replaced with a 32-bit number uniform in the interval from -1 to 1 . This modification facilitated the use of a fast random number generator, RCAR-RY,¹¹ having a very long period of approximately 2^{1407} . The needed diffusion coefficient of 1.35×10^{-5} $\text{cm}^2 \text{sec}^{-1}$ was obtained using a multiplicative scaling factor. A time step, Δt , of 60 ps was used. Simulations of 0.5 ms required approximately 5 days on an Apple G4 450 MHz computer. We have found that this algorithm faithfully models a wide variety of electrochemical experiments at flat electrode surfaces (where comparisons with analytical equations are possible).

Whereas our previous simulations were all conducted under conditions of diffusion control, we have developed a scheme for simulating Nernstian electrodeposition reactions at rates below diffusion control here. Briefly, a "Nernst layer" 20 nm in thickness and bounded by the electrode surface at one end was defined as shown in Scheme 2. Within this Nernst layer, the concentration of metal ions was adjusted to equal that predicted by the Nernst equation:

$$C_{\text{Nernst}} = \exp\left[\frac{F(\eta_{\text{dep}} + E_{\text{eq}})}{RT}\right] \quad (3)$$

The concentration within the Nernst layer was adjusted to C_{Nernst} by iteratively changing the probability of reaction, p , for ions colliding with metal particles on the surface. The number of ions in the Nernst layer was assessed each time step (60 ps), and p was incremented by 0.01 (+0.01 if a surplus of ions was present; -0.01 if a deficit of ions was present). A reactive collision of an ion with a particle caused all of the following to occur: 1. That ion was removed from the simulation; 2. The hemispherical particle involved in the collision increased in volume by an increment equal to that of a single silver atom, and; 3. An electron was added to the tally for that simulation time increment. The formation of metal adatoms (e.g., by discharge of silver ions on the electrode surface away from nuclei) was not permitted. This boundary condition at $z = 0$ closely models the behavior of highly oriented pyrolytic graphite in our experiments.

The Nernst layer construct requires silver nanoparticles everywhere on the electrode surface to respond simultaneously to an "error" in C_{Nernst} . This might seem, at first, to be an unphysical approximation. However, in the case of a graphite electrode surface, this approximation is justified by the fact that the potential of the solution at the electrode surface can be detected everywhere on the electrode surface (by the graphite surface and by the metal particles present on its surface). If, instead, the supporting surface were incapable of sensing the potential of the contacting solution, and this potential could be detected only at the metal particles, this approximation would not be justified.

The performance of this algorithm was checked by simulating the electrodeposition of silver at a flat silver electrode surface. Results for eight deposition potentials are shown in Figure 2. In Figure 2a are plotted charge versus time transients. These transients are linear in time ($t^{1/2}$), as shown in the Anson plots of Figure 2b and as predicted by a form of the integrated Cottrell equation:

$$Q(t) = \frac{2FAD^{1/2}t^{1/2}}{\pi^{1/2}}[C^* - C_{\text{Nernst}}] \quad (4)$$

The slopes obtained from the Anson plot are compared with the slopes predicted by eq 4 in Figure 2c and good agreement is obtained.

III. Results and Interpretation

Shown in Figure 3a are current versus time transients for electrodeposition experiments conducted at η_{dep} values of -1, -20, and -200 mV. In the inset of this figure, the same current transients are plotted as a function of time^{-1/2}. The solid lines in this inset are the predictions of the Cottrell equation, and good agreement with the Brownian dynamics data are seen. In Figure 3b the mean particle radius, $\langle r \rangle$, is plotted as a function of time for six values of η_{dep} . Qualitatively, as expected, the

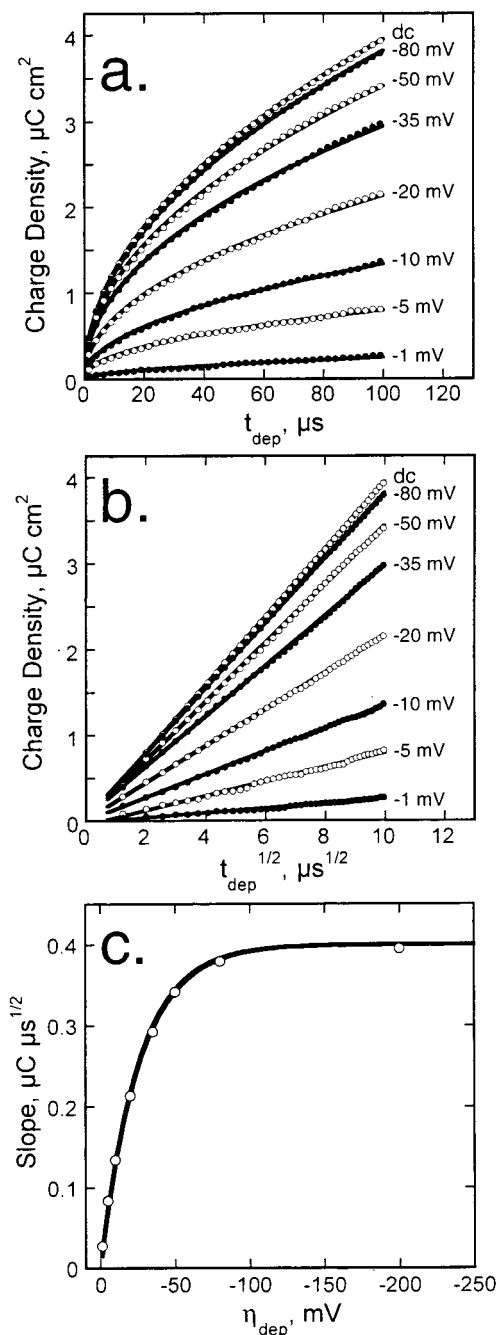


Figure 2. Simulation results for the electrodeposition of silver from a 1.0 mM solution at a planar electrode using eight values of η_{dep} as indicated: (a) charge versus time transients, (b) Anson plots of charge versus time^{1/2}, and (c) plot of the slopes of the Anson plots versus η_{dep} . The solid line is the prediction of eq 3. The simulation-to-simulation reproducibility of Q (i.e., $\pm \sigma_Q$) was smaller than the diameters of the symbols.

rate of growth for metal particles decreases with η_{dep} . In contrast to the situation for an isolated metal nucleus growing at diffusion control (where $r \propto t^{1/2}$), however, the dependence of $\langle r \rangle$ on time is not described by a simple power law at any of the deposition potentials investigated here. This conclusion follows the observation that the log $\langle r \rangle$ vs log t plots of Figure 3c exhibit curvature over the entire range of $\langle r \rangle$.

The most important result of this study relates to the data presented in Figure 4. In Figure 4a and b, the standard deviation of the particle radius, σ_r , is plotted as a function of $\langle r \rangle$. These plots provide a direct comparison of the rates at which size dispersion increases as a function of $\langle r \rangle$ for a particular ensemble

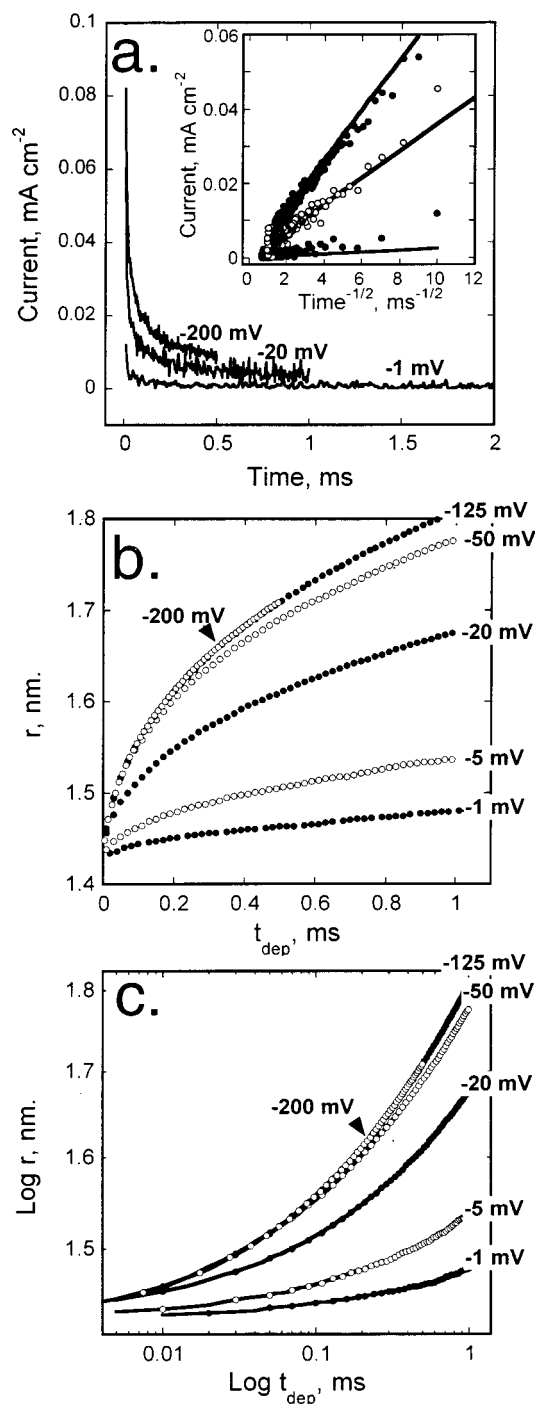


Figure 3. (a) Current versus time transients for the growth of the 200 particle ensemble at three potentials: -200 , -20 , and -1 mV. Inset: Plots of current versus time^{-1/2} for these data. (b) Mean particle radius versus t_{dep} for simulations at six η_{dep} as indicated. (c) Log $\langle r \rangle$ vs Log t_{dep} plots for the same data shown in (b).

of silver particles undergoing growth at six different deposition rates. Shown in Figures 4a and b are error bars that indicate the simulation-to-simulation reproducibility of these data for three simulations at each value of η_{dep} each conducted with a different plating "solution". The salient features of these data may be summarized as follows: All six plots are approximately linear, all possess a positive slope, and the slope at each potential is *significantly* different (when the simulation-to-simulation dispersion of the data are considered). Moreover, as shown in Figure 4c, the slopes of the σ_r versus $\langle r \rangle$ data, $d\sigma_r/dr$, increase with increasing η_{dep} . These data support the conclusion that slow

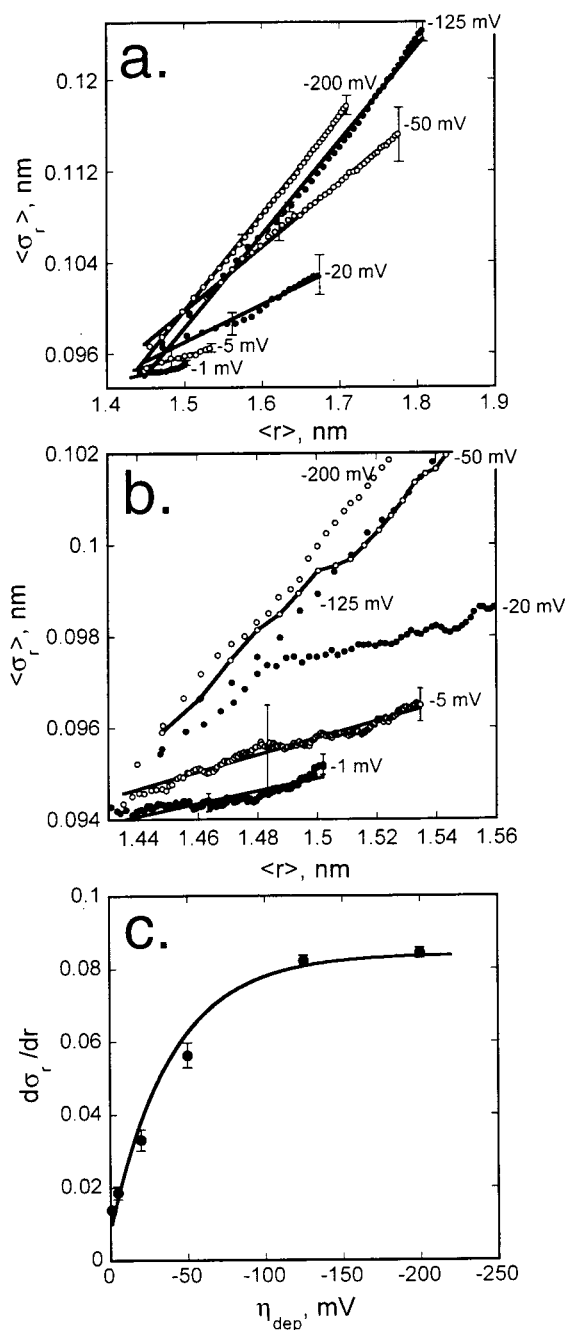


Figure 4. (a) Standard deviation of the particle radius, σ_r , versus $\langle r \rangle$ for simulations at six η_{dep} as indicated. Solid lines are the results of linear least-squares analysis for each η_{dep} . The error bars in this plot represent $\pm 1\sigma$ for the σ_r obtained from three or four replicate simulations conducted at each η_{dep} . (b) Mean particle radius versus t_{dep} for simulations at six η_{dep} as indicated. (c) Results of the linear least-squares analysis of the data shown in (a) and (b). The error bars in this plot represent $\pm 1\sigma$ for $d\sigma_r/dr$ obtained from three or four replicate simulations conducted at each η_{dep} .

growth reduces the rate at which size dispersion increases. Since the slope of Figure 4c is steepest at small values of η_{dep} , it can also be concluded that the marginal effect of reducing η_{dep} on this rate is greatest at low overvoltages. Finally, it is apparent that the plot of $d\sigma_r/dr$ versus $\langle r \rangle$ has a positive intercept on the $d\sigma_r/dr$ axis. This suggests that even in the limit of low η_{dep} we are unlikely to achieve convergent growth for an ensemble of metal nanoparticles. These are important predictions that can be tested experimentally.

Why does σ_r increase with $\langle r \rangle$, and why is the rate of this increase related to η_{dep} ? For randomly nucleated ensembles of metal particles growing at diffusion control, our previous Brownian dynamics results⁷ revealed a clear dependence of the growth rate for metal particles on the distance to the closest particle on the electrode surface (henceforth, the nearest neighbor distance or NND). Specifically, the mean rate of growth for two nearest neighbors was inversely related to the NND. This correlation becomes more pronounced as the number density of particles on the surface increases and the NND for particles on the surface decreases.⁶ When this correlation is observed, the rate of growth for the two nearest neighbors is retarded relative to the rate of growth for nanoparticles growing in isolation. This retardation of the growth rate is caused by the overlap of the depletion layers between neighboring particles – a phenomenon we have termed interparticle diffusional coupling. IDC occurs for particles that are randomly positioned on a surface and for particles that are located in a hexagonal array. However, in the latter case, the retardation of the growth rates for nearest neighbors is identical because NND is the same for every particle in the hexagonal array. No increase in σ_r with $\langle r \rangle$ is observed (in fact, growth is weakly convergent⁷). Collectively, these observations support the conclusion that IDC is the *primary* mechanism by which size dispersion is created in randomly nucleated arrays of metal particles when nucleation is instantaneous and deposition is diffusion controlled.

Is there evidence in these simulations that the deleterious effects of IDC are moderated by reducing η_{dep} ? The answer is “yes”. Shown in Figure 5a and b are plots of the normalized growth rate ($\Delta r / \langle \Delta r \rangle$ where $\Delta r = r(t) - r_{\text{initial}}$) for particles as a function of the NND evaluated for simulations carried out at $\eta_{\text{dep}} = -200$ mV (Figure 5a) and -1 mV (Figure 5b). If linear least-squares analysis is used to assign a slope to these plots, both the correlation coefficient R , and the slope of the -200 mV data are greater than the corresponding values for the -1 mV data. We conclude that IDC is more prevalent during deposition at $\eta_{\text{dep}} = -200$ mV as compared with -1 mV. The plot of Figure 5c shows that this trend extends to the growth of the nanoparticle ensemble at other values of η_{dep} as well. Here, R and the slope of the $\Delta r / \langle \Delta r \rangle$ versus the NND are plotted as a function of η_{dep} . Both quantities increase smoothly with η_{dep} , and the shapes of these two curves parallel the shape of the $d\sigma_r/dr$ versus η_{dep} plot of Figure 4c.

Can there be a common explanation for the shapes of these three plots (i.e., those of Figures 4c and 5c)? One possible explanation relates to the *degree* of diffusion layer overlap present in the 200 particle ensemble at each value of η_{dep} . For randomly nucleated metal particles, the overlap of the diffusion layers of neighboring particles occurs gradually as these particles and their associated steady-state diffusion layers (eq 1) increase in size. The relationship between the fraction of nanoparticles where overlap has occurred, θ , and $\langle r \rangle$ can be numerically calculated for a particular spatial arrangement of particles if η_{dep} and C^* are known. This calculation involves a comparison of the quantity $2\langle r \rangle + 2\langle r_d \rangle$ with the NND for each of the 200 particles on the surface (where $\langle r_d \rangle$ is the mean diffusion layer radius). The value for $\langle r_d \rangle$ associated with η_{dep} can be calculated using eqs 2 and 3 if $C_o = C_{\text{Nernst}}$. When this numerical calculation is carried out, an s-shaped relationship between θ and $\langle r \rangle$ is obtained for the 200 particle ensemble of interest in this work. At $\eta_{\text{dep}} = -5$ mV and $C^* = 1.0$ mM, this plot is shown in Figure 6a. In this example, θ increases from 0.1 at $\langle r \rangle = 0.7$ nm to 0.9 at $\langle r \rangle = 3.4$ nm. The increase of θ over this range of $\langle r \rangle$ values is a direct consequence of the dispersion in

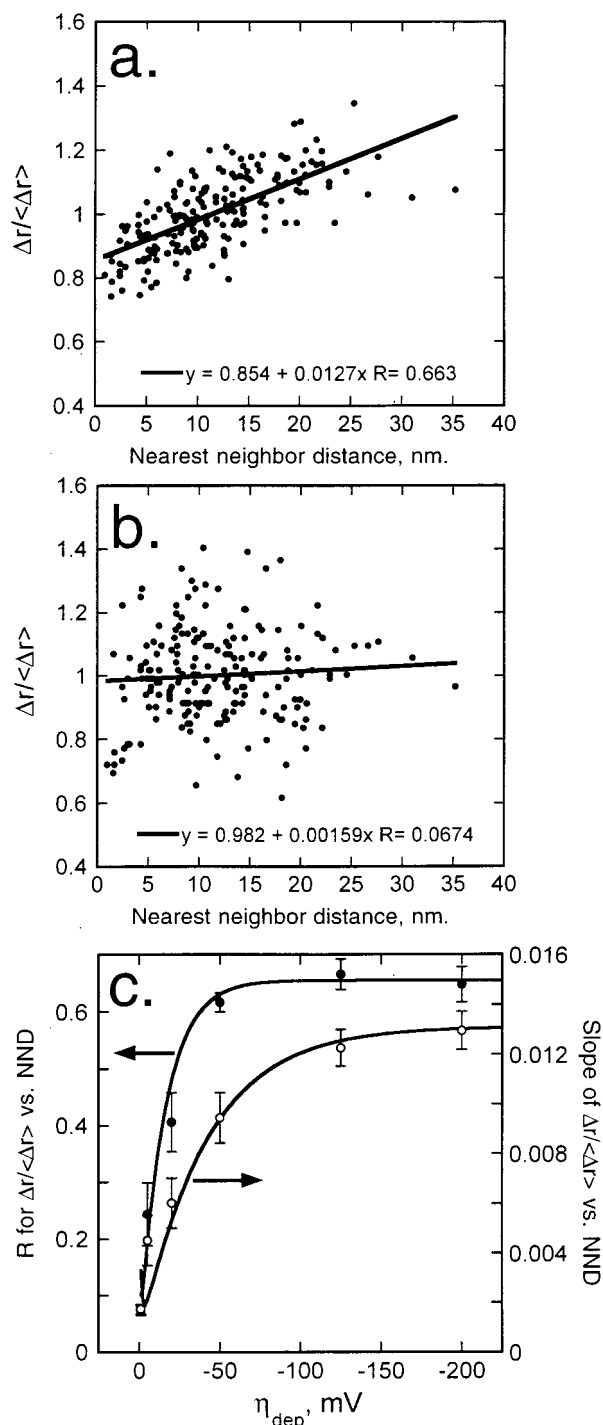


Figure 5. Plots of the normalized growth rate, $\Delta r / \langle \Delta r \rangle$, versus the nearest neighbor distance for two simulations conducted at $\eta_{\text{dep}} = -200$ mV (a) and $\eta_{\text{dep}} = -1$ mV (b). The equations and R values derived from linear least-squares analyses of these data sets are indicated at the bottom of each plot. (c) Plots of the least-squares slope (\circ), and regression coefficient, R (\bullet), versus η_{dep} for all of the data sets collected at the six η_{dep} values. The error bars in this plot represent $\pm 1\sigma$ for the $\Delta r / \langle \Delta r \rangle$ obtained from three or four replicate simulations conducted at each η_{dep} .

the NND (Figure 6b) present in this randomly nucleated ensemble. Relative to this range of $\langle r \rangle$ values, the increase in $\langle r \rangle$ (and therefore of θ) over the course of our 1 ms simulation at $\eta_{\text{dep}} = -5$ mV ($\langle r \rangle_{\text{initial}} = 1.44$ nm; $\langle r \rangle_{\text{final}} = 1.53$ nm) is small. This is equally true for the simulations conducted at other values of η_{dep} . Therefore, to a first approximation, the results of simulation runs at different values of η_{dep} can be interpreted in terms of a particular value of θ .

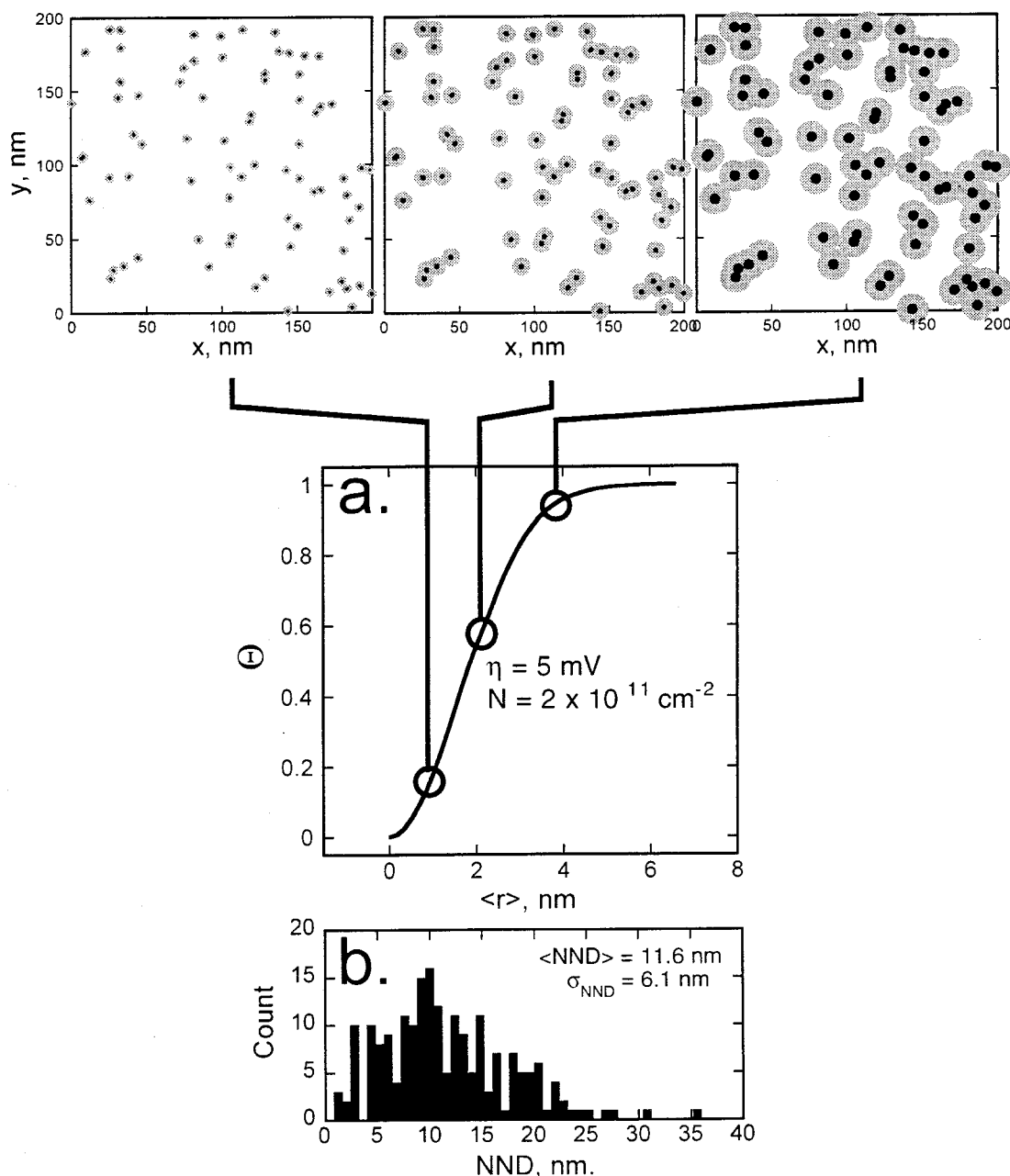


Figure 6. (a) Plot of the fraction of particles for which diffusion-layer overlap with neighboring particles has occurred, Θ , as a function of $\text{Log } \langle r \rangle$. This plot was generated numerically for the 200-particle ensemble that is of interest here, assuming $\eta_{\text{dep}} = -5$ mV. Shown at top is a 200×200 nm region of the electrode surface showing, schematically, the radius of individual particles (shown in black) and the depletion layer surrounding each (shown in gray). (b) Histogram of nearest neighbor distances for the 200-particle ensemble used as the starting point in these simulations.

Shown in Figure 7 are plots of θ versus $\langle r \rangle$ (Figure 7a), and θ versus $\text{Log } \langle r \rangle$ (Figure 7b), for the six η_{dep} values employed in the simulations. Also shown (by dotted lines) are plots for “kinetically controlled” growth. Since under conditions of kinetic control no depletion layer is present ($r_d = 0$), these dotted lines indicate the values for $\langle r \rangle$ at which the surfaces of nearest neighbors will physically touch and these two particles will coalesce into one. Figures 7a and b show that as the deposition rate and $\langle r_d \rangle$ increase, the overlap of diffusion layers occurs at smaller values of $\langle r \rangle$, qualitatively as expected. In Figures 7a and b, the mean particle radius of the 200 particle ensemble used as the starting point in these simulations ($\langle r \rangle_{\text{initial}} = 1.44$ nm) is shown by a vertical line. The values for θ corresponding to this $\langle r \rangle_{\text{initial}}$ are plotted versus η_{dep} in Figure 7c. We see that the simulations performed in this study have spanned θ ranging from 0.05 (at -1 mV) to 1.0 (at -200 mV). Moreover, the shape of this plot mimics that of the plots shown in Figures 4c

and 5c, right down to the nonzero intercepts of these plot on their respective vertical axes. A common explanation for the plots of Figures 4c and 5c can now be proposed: The increase in $d\sigma_r/dr$ with η_{dep} (Figure 4c) and the increases in the two plots of Figure 5c (associated with the prevalence of IDC) are both related to the degree to which diffusional overlap between neighboring particles has taken place. Plots of θ versus $\langle r \rangle$ (or $\text{Log } \langle r \rangle$) can therefore be of significant experimental value. Such plots, which can be readily calculated for any conditions of nucleation density, C^* , and η_{dep} , can be used to predict not only if IDC will contribute the size dispersion of an ensemble of particles having a particular mean radius, but can also be used to estimate the extent to which IDC will pose a problem.

Finally, in Figure 7b it can be seen that the θ versus $\text{Log } \langle r \rangle$ plot for diffusion control (as approximated by $\eta_{\text{dep}} = -200$ mV) is shifted left from the plot for kinetic control by 1 order of magnitude in $\langle r \rangle$. This interval in $\langle r \rangle$ represents the maximum

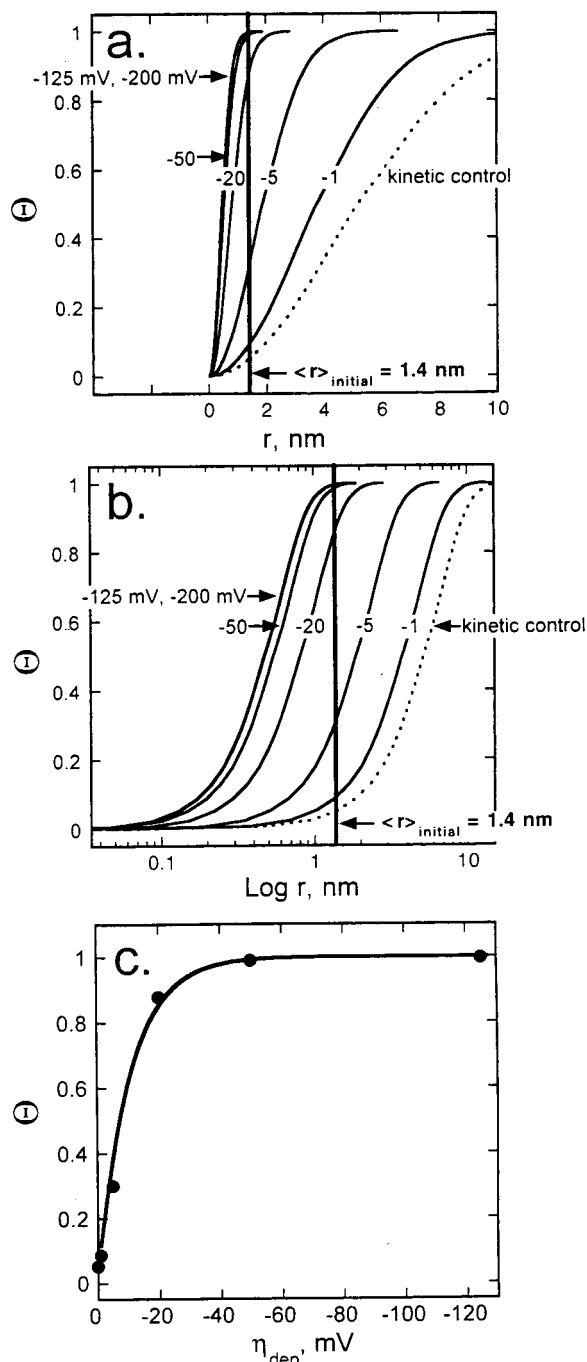


Figure 7. Plots of Θ versus $\langle r \rangle$ (a) and $\text{Log } r$ (b) for six values of η_{dep} . Shown in each plot is the mean radius of the 200-particle ensemble that was used as the starting point for the simulations conducted in this study (1.43 nm). (c) Plot of Θ_{initial} (Θ at $t = 0$) versus η_{dep} for the 200-particle ensemble that was used as the starting point for the simulations conducted in this study.

extent to which slow growth can forestall the onset of the deleterious effects of interparticle diffusional coupling.

IV. Summary

An adaptation of the Brownian dynamics simulation method has been used to model the growth of a particular 200 particle ensemble of silver nanoparticles. This ensemble of particles was randomly positioned on an electrode of total area 1.0×10^{-9} cm^2 (Scheme 2), and these particles possessed a significant size distribution (Figure 1). The growth of this distribution was probed at overpotentials, η_{dep} , ranging from -1 mV to -200 mV. The results of these simulations support the following conclusions.

1. Slow growth works. That is, low deposition overpotentials provide an effective means by which narrower particle size dispersions (narrower by comparison with the distributions obtained for growth at diffusion control) can be obtained in electrodeposition. This conclusion holds provided nucleation is instantaneous at the reduced overpotentials employed for growth.

2. The increase in particle size dispersion seen at all deposition overpotentials is a consequence of interparticle diffusion coupling, IDC. IDC “translates” the distribution in nearest neighbor distances into a distribution in the growth rates for particles on the electrode surface. The growth rate for an individual particle in the ensemble is inversely related to its proximity to other particles.

3. Low deposition potentials are effective because IDC is reduced. IDC is reduced because the radius of the depletion layer surrounding each particle, r_d , is proportional to $C^* - C_o$, and C_o approaches C^* (r_d approaches 0) as η_{dep} approaches 0 V. Since IDC is mediated by the depletion layer, a reduction in η_{dep} translates directly into a reduction in IDC.

4. The effectiveness of slow growth is limited. In fact, there are at least two important limitations. First, slow growth will not be beneficial unless IDC is present. At a sufficiently low nucleation densities, there will be no benefit to growth at low voltages. Second, in cases where IDC is present, slow growth will produce a narrower size distribution than is obtainable at diffusion control, but convergent growth (i.e., decreasing σ_r with $\langle r \rangle$) will never be obtained. In the simulations conducted here, σ_r increased with $\langle r \rangle$ even for $\eta_{\text{dep}} = -1$ mV. The effectiveness of slow growth is related to θ , which can be calculated for experimentally relevant conditions of the nucleation density, η_{dep} , and C^* .

Acknowledgment. The funding of this work by the National Science Foundation (#DMR-9876479) and the Petroleum Research Fund of the American Chemical Society (#33751-AC5) is gratefully acknowledged. The author also gratefully acknowledges an A. P. Sloan Foundation Fellowship and a Camille Dreyfus Teacher–Scholar award.

References and Notes

- (1) Gorer, S.; Ganske, J.; Hemminger, J. C.; Penner, R. M. *J. Am. Chem. Soc.* **1998**, *120*, 9584.
- (2) Hsiao, G.; Anderson, M. G.; Gorer, S.; Harris, D.; Penner, R. M. *J. Am. Chem. Soc.* **1997**, *119*, 1439.
- (3) Nyffenegger, R. M.; Craft, B.; Shaaban, M.; Gorer, S.; Penner, R. M. *Chem. Mater.* **1998**, *10*, 1120.
- (4) Zoval, J. V.; Stiger, R. M.; Biernacki, P. R.; Penner, R. M. *J. Phys. Chem.* **1996**, *100*, 837.
- (5) Zoval, J. V.; Lee, J.; Gorer, S.; Penner, R. M. *J. Phys. Chem.* **1998**, *102*, 1166.
- (6) “Instantaneous” nucleation refers to a situation in which the time interval during which nucleation occurs is much shorter than the subsequent particle growth phase.
- (7) Fransaer, J.; Penner, R. M. *J. Phys. Chem. B* **1999**, *103*, 7643.
- (8) Liu, H.; Penner, R. M. *J. Phys. Chem. B* **2000**, *104*, 9131.
- (9) Liu, H.; Favier, F.; Ng, K.; Zach, M. P.; Penner, R. M. *Electrochim. Acta* **2001**, in press.
- (10) Ermak, D. L.; McCammon, J. A. *J. Chem. Phys.* **1978**, *69*, 1352.
- (11) Marsaglia, G.; Narasimhan, B.; Zaman, A. *Comput. Phys. Commun.* **1990**, *60*, 345.
- (12) R is the square root of the coefficient of determination; often used to express the degree to which a regression line predicts the actual Y vs X data. A formal definition of R is

$$R = \frac{S_{XY}}{\sqrt{S_X S_Y}}$$

where $S_{XY} = \Sigma(X - \langle X \rangle)(Y - \langle Y \rangle)$; $S_{XX} = \Sigma(X - \langle X \rangle)^2$; $S_{YY} = \Sigma(Y - \langle Y \rangle)^2$. See, for example, Sachs, L. *Applied Statistics: A Handbook of Techniques*, 2nd ed.; Reynarowych, Z., trans.; Springer-Verlag: New York, 1984; Academic Press: New York.